NeuroImage 340 (2026) 122238

Contents lists available at ScienceDirect

NeuroImage

journal homepage: www.elsevier.com/locate/ynimg

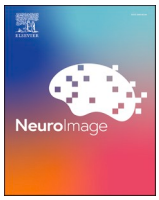

Training-induced brain network reorganization predicts location specificity and transfer in perceptual learning

Lin Zhong [a], Gong-Liang Zhang [b], Jun-Yun Zhang [c], Cong Yu [a,*]

[a] Department of Psychology and Behavioral Sciences, Zhejiang University, Hangzhou, China
[b] Department of Psychology, Soochow University, Suzhou, China
[c] School of Psychological and Cognitive Sciences, Peking University, Beijing, China

ARTICLE INFO

Keywords:
Visual perceptual learning
Brain network reorganization
Learning transfer

ABSTRACT

Visual perceptual learning is often highly specific to the trained retinal location, a hallmark observation that is traditionally interpreted as evidence that training-induced plasticity occurs in retinotopic early visual cortex. However, under properly designed training conditions, such as double training, adaptation prevention, and attention modulation, learning can transfer fully to untrained locations, challenging this classical view and raising the question of what determines whether learning remains specific or generalizes. Here, we analyzed EEG data from a Vernier learning task in which some participants showed strong location specificity while others exhibited robust interhemifield transfer. Time-frequency analyses revealed post-training beta-band suppression in location-specific learners, but not in transfer learners. Graph-theoretic analyses further showed that location specificity was associated with increased clustering and longer shortest path lengths, indicating stronger local segregation and reduced global integration. In contrast, learners who transferred maintained a comparatively stable network organization. These findings provide a systems-level account of learning specificity and transfer, with implications extending beyond visual perception to other domains of skill acquisition.

1. Introduction

Perceptual learning refers to the long-term improvement in sensory discrimination following intensive practice. Classic psychophysical studies show that learning can be highly specific to trained stimulus features, such as orientation, spatial frequency, and retinal location (Crist et al., 1997; Fahle, 1994; Fiorentini and Berardi, 1980; Karni and Sagi, 1991; Schoups et al., 1995; Yu et al., 2004). Location specificity has played a particularly important role in theories of perceptual learning because it has often been interpreted as evidence that training induces plasticity in early retinotopic visual cortex (Ahissar and Hochstein, 1997; Crist et al., 1997; Fahle, 1994; Karni and Sagi, 1991; Schoups et al., 1995).

Yet, learning can transfer substantially or completely to untrained retinal locations with double training (Mastropasqua et al., 2015; Wang et al., 2013, 2012, 2014; Xiao et al., 2008; Xiong et al., 2016). For example, location-specific contrast-discrimination learning could transfer completely to an untrained retinal location when contrast-discrimination training was paired with orientation-discrimination training at the transfer location (Xiao et al., 2008). Related findings show that adaptation prevention (Harris et al., 2012) and attention modulation (Donovan and Carrasco, 2018; Donovan et al., 2015) can also promote learning transfer to new locations. These findings challenge the view that perceptual learning is confined to low-level sensory plasticity and instead point to higher-level mechanisms. Accumulating evidence suggests that perceptual learning may reflect the acquisition of abstract sensory rules or concepts, rather than retinotopically bound sensory changes (Hu et al., 2021; Wang et al., 2016; Xiong et al., 2022; Zhang et al., 2010).

Despite this progress, a fundamental question remains unresolved: why is perceptual learning location-specific in the first place, and what determines whether learning generalizes or remains location-specific? Two prominent hypotheses have been proposed. The connection-failure hypothesis proposes that learning remains specific when higher-level learning mechanisms cannot effectively access sensory inputs from an untrained location (Wang et al., 2012; Xiao et al., 2008; Xiong et al., 2016). Supporting this view, Zhang et al. (2013) reported that ERP P1/N1 modulations at the untrained location emerged only in participants who transferred, whereas their absence in location-specific learners was consistent with impaired communication between

* Corresponding author.
E-mail address: yu_cong@zju.edu.cn (C. Yu).

https://doi.org/10.1016/j.neuroimage.2026.122238
Received 7 May 2026; Received in revised form 14 September 2026; Accepted 14 September 2026
Available online 15 September 2026

higher-level learning mechanisms and early visual representations of the untrained location. The overfitting hypothesis, in contrast, proposes that practice can produce excessive tuning to task-relevant and incidental features of the trained condition, resulting in strong but inflexible learning (Mollon and Danilova, 1996; Sagi, 2011). Although these accounts emphasize different mechanisms, both suggest that learning specificity may reflect an imbalance between local specialization and the capacity of distributed brain systems to communicate beyond the trained condition.

Graph theory provides a framework for testing this possibility. Functional brain networks can be represented as graphs in which recording sites are nodes and functional interactions are edges. The clustering coefficient measures how strongly neighboring nodes are interconnected and therefore indexes local segregation or specialization. In contrast, path length measures the average shortest route between nodes, with longer paths indicating less efficient global integration and distributed communication (Achard and Bullmore, 2007; Rubinov and Sporns, 2010; Sporns, 2013; Watts and Strogatz, 1998). These measures have been widely used to quantify network differences associated with cognitive and affective states, and to characterize alterations in large-scale network organization in clinical populations, including ADHD and Alzheimer's disease (Aydın, 2024; Aydın et al., 2022; Aydin and Onbasi, 2024). In this context, overfitting as a hypothesized mechanism for specificity may be reflected at the network level in stronger local clustering, whereas connection failure may be reflected in longer path length and reduced global integration. Together, these changes would be consistent with a shift toward stronger local segregation relative to distributed communication.

Electroencephalography (EEG) is well suited to examining functional network organization. In the present sensor-level networks, electrodes were treated as nodes and functional interactions between electrodes as edges. Functional connectivity can be quantified using phase-locking value (PLV), which measures the consistency of phase differences between EEG signals across trials and provides an index of frequency-specific interelectrode synchronization (Lachaux et al., 1999). Pairwise PLV can therefore define functional network edges for examining local segregation and distributed integration. Because oscillatory interactions across frequency bands are associated with distinct modes of neuronal coordination and cognitive processing (Siegel et al., 2012), frequency-resolved PLV analysis provides a useful approach for characterizing the neural dynamics of perceptual learning.

However, direct neural evidence that perceptual-learning specificity reflects an imbalance between local specialization and distributed communication is missing. In our previous ERP study using the same Vernier-learning dataset (Zhang et al., 2013), training-related P1/N1 changes at the untrained location were observed only in participants who showed behavioral learning transfer, whereas learners whose learning remained location-specific showed P1/N1 changes primarily at the trained location. These findings suggested that learning transfer may depend on whether learning-related changes extend beyond the trained retinal representation, but the ERP analysis did not address how learning reorganizes large-scale functional connectivity.

In the current study, we reanalyzed these EEG data using graph-theoretical analysis. We hypothesized that transfer and location specificity would show distinct training-related changes in network organization, reflected in the balance between local segregation and distributed integration. Specifically, we expected location specificity to be associated with a shift toward stronger local segregation relative to distributed integration, whereas transfer would be associated with greater preservation of this balance. By examining these complementary network dimensions, we aimed to provide a systems-level account of the neural processes associated with specificity versus transfer in perceptual learning, with broader implications for understanding learning generalization.

2. Methods

The raw data from a previous study of ours (Zhang et al., 2013) were re-examined in this study. Details concerning the participants and the psychophysical task are also included here for reference.

2.1. Participants

Twenty-eight right-handed healthy participants (13 male and 15 female undergraduate students; 20.28 ± 2.26 (SD) years) with normal or corrected-to-normal vision participated in this study. Informed consent was obtained from all participants prior to data collection. The research protocol received approval from Beijing Normal University Institutional Review Board.

2.2. Psychophysical task

Participants performed a Vernier discrimination task. The Vernier stimulus (Fig. 1A) consisted of two identical Gabor patches displayed on a mean luminance background. Each trial began with a foveal fixation cross ($0.25^\circ \times 0.25^\circ$) presented for 500 ms, which remained visible throughout the trial. The Vernier stimulus was then displayed for 200 ms, and participants judged whether the upper Gabor was offset to the left or right of the lower Gabor. These Gabors were presented at the center of the lower-left or lower-right visual quadrant (5° retinal eccentricity), shared the same spatial frequency (3 cpd), standard deviation (0.48°), contrast (0.45), orientation (vertical), phase (90°), and had a center-to-center separation of 1.67°. The upper Gabor was horizontally displaced relative to the lower Gabor by the Vernier offset, perpendicular to their orientation. Vernier alignment thresholds were measured using a single-interval two-alternative forced-choice (2AFC) paradigm. Thresholds were determined by adjusting the Vernier offset to converge at a threshold level of 4.53 ± 0.26 arcmin (mean $\pm$ SE).

The task comprised seven sessions, including a baseline behavioral and EEG recording session (S1), four behavioral training sessions (S2-S5), an EEG post-training session (S6), and a final behavioral post-training session (S7) (Fig. 1B). Training was always performed in the lower-left visual quadrant, while pre- and post-training assessments were conducted in both the trained (lower-left) and untrained (lower-right) quadrants. Each EEG session (S1, S6) comprised multiple 250-trial blocks, and each behavioral training session (S2-S5) comprised 125-trial blocks. Brief rest breaks were provided every 42 trials to minimize fatigue. Auditory feedback was provided after incorrect responses during all behavioral staircase trials, including the behavioral baseline assessment in S1, the training sessions S2–S5, and the post-training behavioral assessment in S7. No auditory feedback was provided during EEG recording trials in S1 or S6.

We computed threshold improvements at the trained and untrained locations, and then calculated a transfer index (TI), defined as the ratio of the percentage improvement at the untrained location over that at the trained location (TI = 0 indicates no transfer; TI = 1 indicates complete transfer). Participants were divided into a transfer group ($n = 14$, TI > 0.5) and a specificity group ($n = 14$, TI ≤ 0.5) for all subsequent analyses (Fig. 1C and D).

2.3. EEG recording and preprocessing

EEG signals were acquired through a NeuroScan recording system (Neurosoft, Inc., Sterling, VA, USA) equipped with 64 Ag-AgCl electrodes arranged on an elastic cap following the international 10–20 system. Neural activity was amplified and continuously sampled at 1000 Hz, with an analog bandpass filter of 0.05–100 Hz. Horizontal EOG was recorded from bipolar electrodes placed at the outer canthi, and vertical EOG was recorded from electrodes placed above and below the left eye. The EEG was referenced online to the left mastoid, and electrode impedances were kept below 5 kΩ.

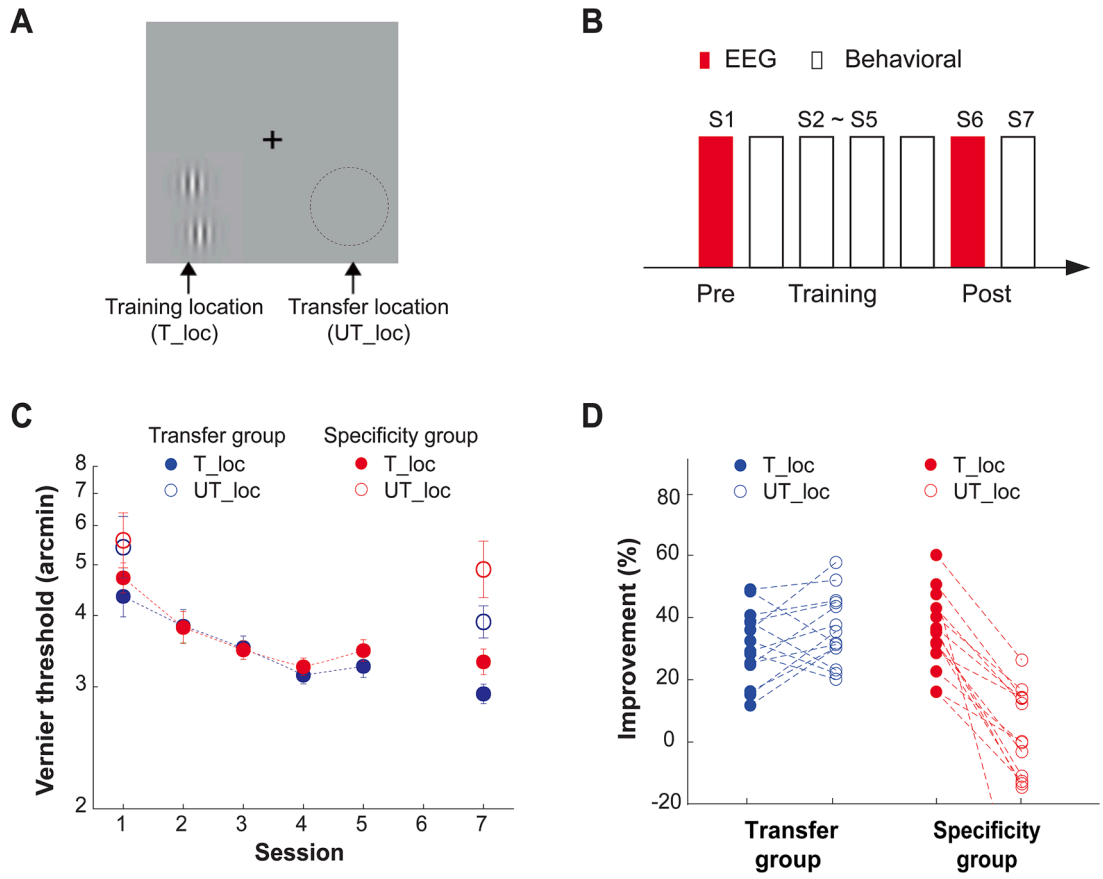

Fig. 1. A. Vernier stimuli. **B**. Training procedure. S1 and S7 assessed pre- and post-training Vernier thresholds. S1 and S6 involved pre- and post-training EEG recordings. S2-S5 were Vernier training sessions. **C**. The learning curves at the trained location and the pre- and post-training thresholds at the untrained location for transfer and specificity groups. **D**. Individual Vernier improvements at the trained and transfer locations for both groups.

Continuous EEG data were first digitally bandpass-filtered (0.5–100 Hz), and notch-filtered at 50 Hz to suppress line noise. Data were preprocessed in EEGLAB 2025.0.0 (Delorme and Makeig, 2004) with custom MATLAB scripts. Independent component analysis (ICA) was applied using EEGLAB's *runica* algorithm, and artifactual components were identified via visual inspection of their temporal, spatial, and spectral features and removed. Noisy channels were reconstructed using spherical spline interpolation (Perrin et al., 1989). Then data were re-referenced to the common average.

2.4. Time-frequency analysis

Epochs from −200 to 600 ms relative to stimulus onset were analyzed using complex Morlet wavelet convolution (van Driel et al., 2017). Wavelet frequencies ranged from 1 to 100 Hz in 0.02 log steps. To balance spectral and temporal precision across frequencies, we used longer wavelets at lower frequencies and shorter wavelets at higher frequencies, since lower frequencies benefit from longer windows and higher frequencies require shorter windows for adequate temporal resolution (Bruns and Eckhorn, 2004; Cohen, 2014). Accordingly, we used 7 cycles for 1–4 Hz, 5 cycles for 4–30 Hz, and 3 cycles for frequencies above 30 Hz. For each trial, power was computed as the squared magnitude of the complex wavelet coefficients, followed by baseline correction using decibel normalization:

$$\text{Power}_{dB} = 10\log_{10}\left(\frac{\text{power}}{\text{baseline}}\right)$$

where for each channel and frequency, the condition averaged power during an interval of −200 to 0 ms relative to the stimulus onset served as baseline activity.

2.5. Graph theoretical analysis

The beta band was selected for connectivity analysis based on the preceding broad-band time-frequency analysis, which examined 1–100 Hz activity and identified significant training-related changes in the beta range (13–30 Hz). Subsequent PLV and graph-theoretical analyses therefore focused on this frequency band. For connectivity and graph-theoretical analyses, the preprocessed EEG data were downsampled to 250 Hz, corresponding to a 4-ms sampling interval. Instantaneous phase at the beta frequency band was obtained from the complex Morlet wavelet coefficients using the same wavelet parameters described above. PLV was computed between all electrode pairs at each time sample and frequency by quantifying the consistency of phase differences across trials. PLV was defined as:

$$PLV = \left|\frac{1}{N}\sum_{n=1}^{N} e^{i\Delta\varnothing_n(t,f)}\right|$$

where $\Delta\varnothing_n(t,f)$ was the phase difference between two electrodes at time t and frequency f for trial n, and N was total trial count. PLV ranged from 0 (random phase relations) to 1 (perfect phase locking), with values closer to 1 indicating more consistent phase relationships and therefore stronger interelectrode phase synchronization (Lachaux et al., 1999).

PLV values were then averaged across 13–30 Hz to obtain a beta-band connectivity matrix at each time point. For the summary graph analysis, these time-resolved connectivity matrices were further averaged across the 0–600-ms task period, yielding one connectivity matrix for each participant and experimental condition. Because the present study focused on how perceptual learning alters coordinated activity across distributed neural signals rather than activity at individual

electrodes alone, PLV was used as the functional connectivity measure for network construction. Each electrode was treated as a node and the PLV between each electrode pair as the edge weight, providing the connectivity matrices used for subsequent graph-theoretical analyses of local segregation and distributed integration.

To characterize whole-brain network reorganization, functional connectivity matrices were first constructed from PLV values and converted into binary adjacency matrices using GRETNA (Wang et al., 2015) across a fixed proportional sparsity range of 0.10 - 0.20 in 0.01 steps, consistent with previous graph-theoretical studies using this range to maintain network reachability while preserving a sparse network topology (Cai et al., 2019; Garrison et al., 2015). Rather than relying on a single sparsity threshold, graph metrics were computed across the entire range and summarized using area-under-the-curve (AUC) measures, providing an integrated measure of network topology across thresholds and reducing dependence on any individual threshold. Two global network metrics were evaluated according to the classical definitions (Watts and Strogatz, 1998):

(1) The clustering coefficient (C) quantified the probability of interconnectedness among neighboring nodes and was defined as

$$C = \frac{1}{N}\sum_{i=1}^{N}\frac{2t_i}{k_i(k_i-1)}$$

where N stood for the total number of nodes in the network, k_i the degree of node i, and t_i the number of existing connections among the neighbors of node i.

(2) characteristic path length (L) measured the average shortest distance between any node pairs and was defined as

$$L = \frac{1}{N(N-1)}\sum_{i\neq j} d_{ij}$$

where d_{ij} represented the shortest path length between nodes i and j, computed as the minimal number of edges that must be traversed to connect them.

To quantify regional reorganization within posterior visual areas, weighted connectivity networks were first constructed by applying the same sparsity thresholds (0.10 - 0.20) used in the whole-brain analysis. The parieto-occipital subnetwork (P1/3/5/7, PO3/5/7, O1, CP1/3/5 and their contralateral counterparts) was then extracted from these sparsity-thresholded matrices. Weighted graph metrics were computed at each sparsity level and summarized using AUC. All subnetwork extraction and computations were implemented in R using custom scripts. Within this subnetwork, we computed two AUC regional network measures:

(1) The average connection strength (Rubinov and Sporns, 2010)

$$\overline{W} = \frac{1}{E}\sum_{(i,j)\in E} w_{(i,j)}$$

where $\overline{W}$ denoted the average of edges within the subnetwork, E was the total number of existing edges, and $w_{(i,j)}$ was the PLV weight between nodes i and j, with higher values indicating stronger average phase synchronization among its nodes.

(2) The average weighted clustering coefficient $\overline{C^w}$ (Onnela et al., 2005), defined as

$$C_i^w = \frac{1}{k_i(k_i-1)}\sum_{j,h}\left(w_{ij}w_{ih}w_{jh}\right)^{\frac{1}{3}},\ \overline{C^w} = \frac{1}{N}\sum_{i=1}^{N} C_i^w$$

where k_i was the degree of node i in the subnetwork, and each term $\left(w_{ij}w_{ih}w_{jh}\right)^{\frac{1}{3}}$ represented the geometric mean weight of a closed triangle connecting nodes i, j and h. N was the number of nodes, with C^w reflecting the tendency of a node's neighbors to be mutually interconnected, weighted by connection strength, thus capturing the density of strongly interconnected triads in the subnetwork.

2.6. Statistics

For each combination of group and location, separate cluster-based permutation tests were conducted to compare pre- versus post-training power modulations using the FieldTrip toolbox (Oostenveld et al., 2011). The analysis focused on posterior electrodes PO3/4/5/6/7/8 and O1/2 for their established sensitivity to visual processing effects (Di Russo et al., 2002). Baseline-normalized power (dB) was subjected to paired-samples t-tests ($\alpha = 0.05$, two-tailed) at each time-frequency point (−200 - 600 ms; 1 - 100 Hz). Clusters were defined as contiguous time-frequency regions exceeding the clustering-forming threshold ($p < 0.05$). Cluster-level statistics were evaluated using the maximum sum of t-values (maxsum) across 2000 random sign-flip permutations. The resulting permutation distribution was used to determine cluster significance, with cluster-level significance determined when observed t-sums exceeded the 95th percentile of permuted data (Maris and Oostenveld, 2007).

For global and subnetwork metrics, a linear mixed-effects (LME) model using the *lmer* function from the "lme4″ package (Bates et al., 2015) treated network metrics as dependent variables. For global network metrics, Group (Transfer vs. Specificity), Location (Trained vs. Untrained), and Training (pre- vs. post-training) were included as fixed effects in a $2 \times 2 \times 2$ factorial design. For subnetwork metrics, Hemisphere (Left vs. Right in subnetwork) was additionally included as a fixed effect in a $2 \times 2 \times 2 \times 2$ factorial design. Participant-specific variability was modeled using random intercepts, and candidate models were compared using likelihood ratio tests to determine whether random slopes for within-subject factors improved model fit. Fixed effects were evaluated within the best-fitting model using F- and t-tests with degrees of freedom estimated via the Kenward-Roger approximation, as implemented in the "lmerTest" package (Kuznetsova et al., 2017). Post hoc analyses were performed using the "emmeans" package (Lenth and Piaskowski, 2025) with Bonferroni correction.

3. Results

3.1. Psychophysics

Twenty-eight right-handed adults completed seven experimental sessions (S1-S7) (Zhang et al., 2013). The Vernier discrimination task was always trained in the lower-left visual quadrant at 5° retinal eccentricity (T_loc), and the transfer effect was measured at the untrained mirror location in the opposite visual hemifield (UT_loc) (Fig. 1A). Pre- and post-training thresholds were measured at both trained and untrained locations in S1 and S7, while pre- and post-training EEGs were recorded in S1 and S6, respectively (Fig. 1B). Training was performed in S2-S5.

A mixed-design ANOVA analysis of threshold improvement with Group as a between-subject factor and Location (trained vs. untrained) as a within-subject factor revealed significant main effects of Group ($F(1, 26) = 14.82$, $p < 0.001$, partial $\eta^2 = 0.36$) and Location ($F(1, 26) = 20.84$, $p < 0.001$, partial $\eta^2 = 0.45$), as well as a significant Group × Location interaction ($F(1, 26) = 36.42$, $p < 0.001$, partial $\eta^2 = 0.58$). Post hoc analysis with Bonferroni correction showed no group difference in improvement at the trained location ($t(26) = -0.92$, $p = 0.733$, *Cohen's d* = 0.33), while at the untrained location, the transfer group exhibited significantly greater improvement than the specificity group ($t(26) = 5.95$, $p < 0.001$, *Cohen's d* = 2.90).

3.2. Time-frequency analysis

We examined the neural dynamics differences between pre-training and post-training for transfer and specificity groups using time-frequency analysis. To identify training-induced EEG modulations, we

computed spectral power on a subset of posterior electrodes (PO3/4/5/6/7/8 and O1/2), which were selected based on previous research suggesting their sensitivity to visual processing (Di Russo et al., 2002; Ding et al., 2006; Mangun and Hillyard, 1991). Cluster-based permutation tests revealed different plasticity patterns: while the transfer group showed no significant power changes ($p > 0.05$) at either location and across all frequency bands (1–100 Hz), the specificity group exhibited a beta-band (13–30 Hz) power reduction approximately 100 ms post-stimulus at both trained and untrained locations ($p < 0.05$, cluster-corrected; Fig. 2A-B). Additional computations on frontal electrodes F1, F2, and Fz revealed no significant changes after training in both transfer and specificity groups (Fig. A1).

3.3. Graph metrics

We next focused on the beta frequency range to examine how training shaped large-scale functional connectivity, thereby providing a network-level perspective on the observed oscillatory plasticity. We constructed beta-band PLV functional connectivity matrices for each pair of electrodes across the entire task period from 0 - 600 ms. The matrices were subsequently binarized across a fixed sparsity range to allow graph-theoretical characterization. We focused on two global network measures: the average clustering coefficient (aC), which indexes segregation and reflects the specialization of localized processing, and the average shortest path length (aL), which indexes integration and reflects the efficiency of distributed information transfer across regions (Sporns, 2013). We first examined whether global network properties changed dynamically with stimulus presentation. The results indicated that aC and aL remained relatively stable throughout the entire 0 - 600 ms interval (Fig. 3A-B). Specifically, to test the pre vs. post differences of aC and aL (0 - 600 ms binned every 4 ms), we applied cluster-based permutation tests for each Group (transfer or specificity) × Location (trained or untrained) condition (1000 permutations). For the transfer group, no significant temporal clusters (e.g., no significant pre vs. post changes) emerged at either the trained or untrained location (cluster-corrected $p > 0.05$), indicating that global network topology remained unchanged after training. In contrast, the specificity group showed a significant temporal cluster spanning the entire 0 - 600 ms window at both locations for two global metrics (aC: $p \leq 0.031$; aL: $p \leq 0.003$; cluster-corrected), indicating a sustained pre-to-post shift in whole-brain segregation and integration, rather than brief, stimulus-locked modulations. This result indicated that changes in these network measures were not driven by stimulus-locked activity, and were already present at the very beginning of stimulus presentation.

Because of this temporal stability, PLV values were then averaged across the full task period to compute global network metrics, which were then submitted to LME analysis with Training, Group, and Location as fixed effects and Participant as a random intercept. The pre- and post-training changes in aC and aL are shown in Fig. 3C-D. For the average clustering coefficient (aC), the LME analysis revealed a significant main effect of Training ($F(1, 78) = 34.54$, $p < 0.001$, partial $\eta^2 = 0.31$), and a significant two-way interaction between Group and Training ($F(1, 78) = 7.79$, $p = 0.007$, partial $\eta^2 = 0.09$). Post hoc analysis with Bonferroni correction indicated no significant difference between transfer and specificity groups before training ($t(36.2) = 0.36$, $p = 0.722$, *Cohen's d* = 0.17), while the specificity group exhibited a significantly stronger aC than the transfer group after training ($t(36.2) = 2.57$, $p = 0.014$, *Cohen's d* = 1.23). For the average shortest path length (aL), the same LME model analysis revealed a significant main effect of Training ($F(1, 78) = 23.88$, $p < 0.001$, partial $\eta^2 = 0.23$) and a significant interaction between Group and Training ($F(1, 78) = 8.88$, $p = 0.004$, partial $\eta^2 = 0.10$). Post hoc analysis indicated a significant training-induced increase in aL in the specificity group ($t(78) = 5.56$, $p < 0.001$, *Cohen's d* = 1.49), but not in the transfer group ($t(78) = 1.35$, $p = 0.182$, *Cohen's d* = 0.36).

To visualize topological changes in functional architecture, we first derived PLV-based functional connectivity matrices for all eight experimental conditions (Group × Training × Location). To facilitate direct observation of network topology under each condition, we then constructed binary and weighted graphs by thresholding these matrices at a sparsity level of 0.10, retaining the top 10% strongest PLV connections in each network. A sparsity level of 0.10 was used for visualization to

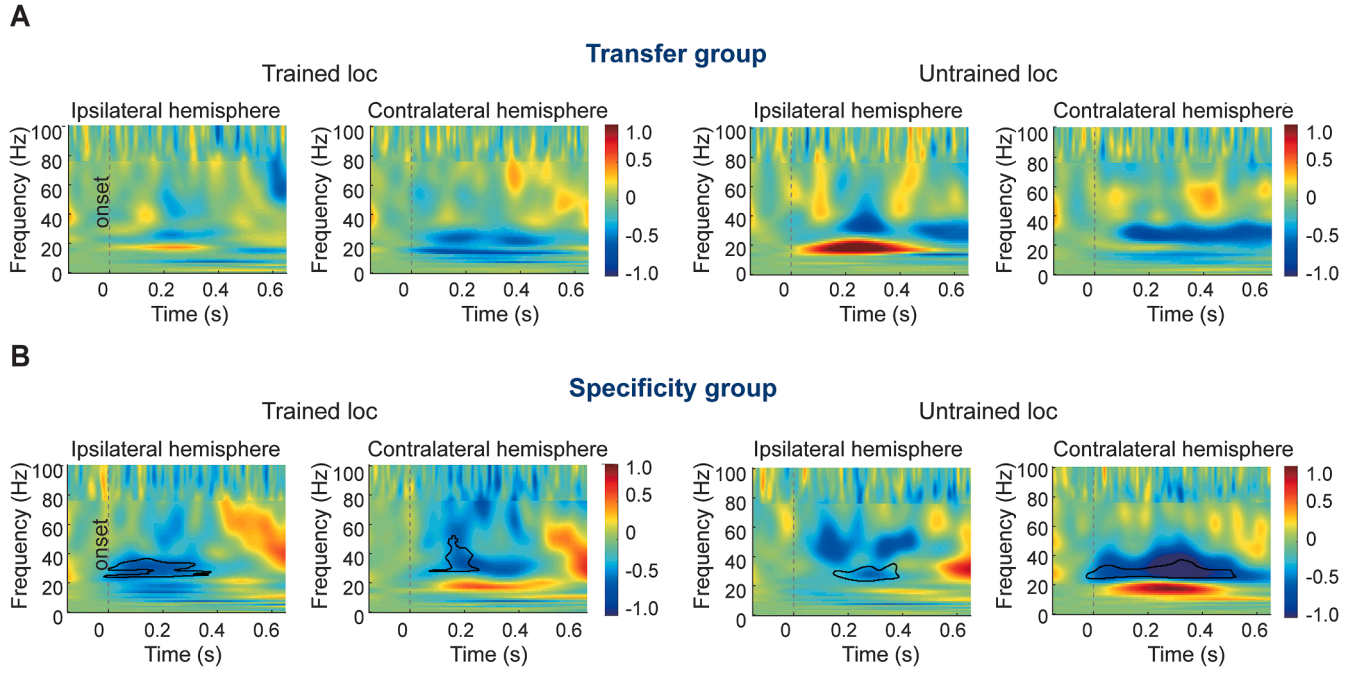

Fig. 2. Time-frequency analysis. **A**. Transfer group. **B**. Specificity group. Time-frequency representations (1–100 Hz) showed post- vs. pre-training power differences in dB over parieto-occipital electrodes (PO3/4/5/6/7/8, O1/2). Vertical dashed lines indicate stimulus onset (0 s). Warm and cool colors indicate power increases and decreases, respectively. Black contours denote clusters that survived cluster-based permutation correction ($p < 0.05$). No significant positive power clusters were detected.

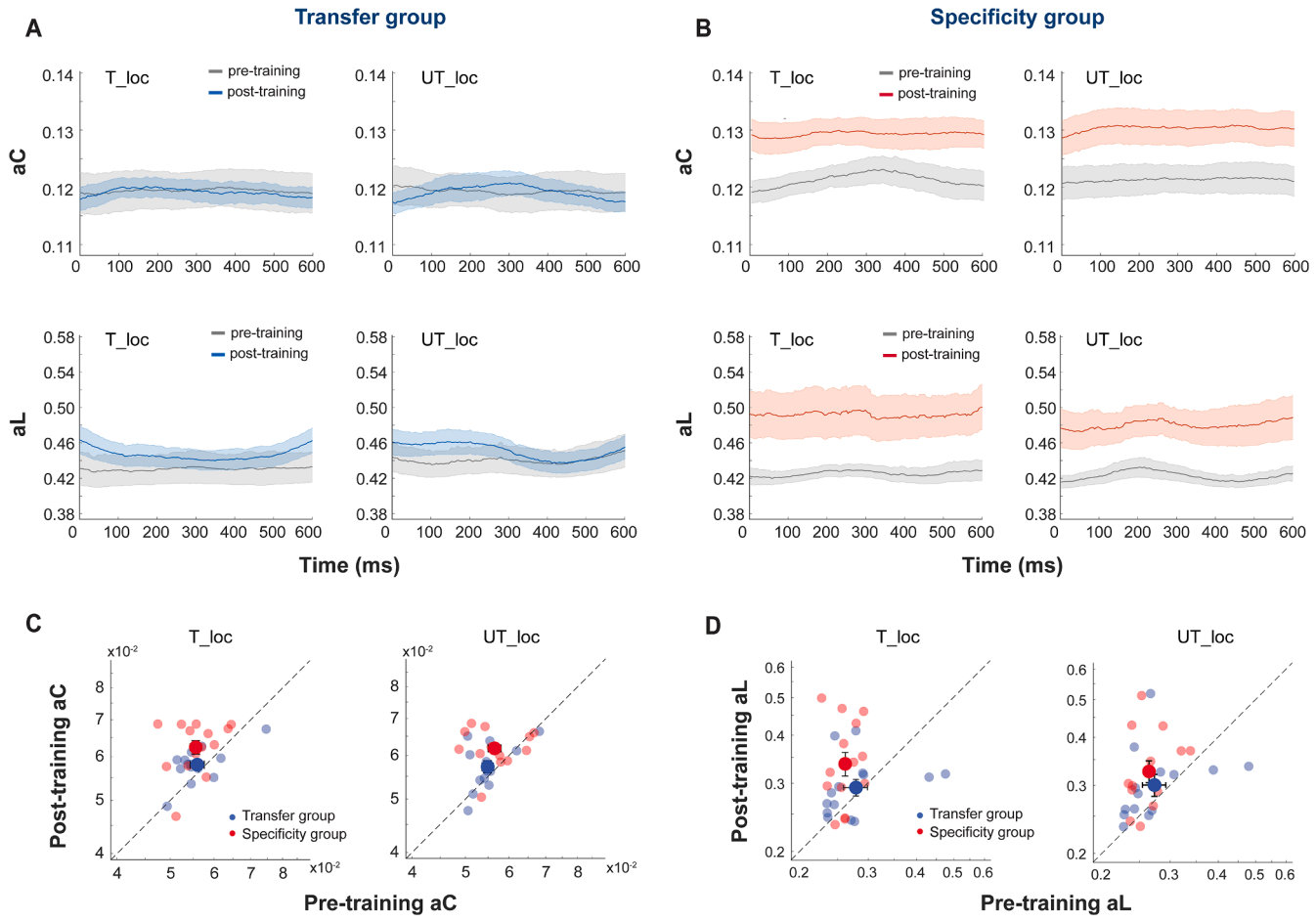

Fig. 3. Global metrics. **A-B**. Time courses (0 - 600 ms post-stimulus) of the average clustering coefficient (aC) and average shortest path length (aL) for the Transfer (A) and Specificity (B) groups, shown separately for the trained and untrained locations. Shaded regions indicate ±1 SEM. **C-D**. Changes in aC and aL. Each light-colored dot represents one participant. Large symbols indicate geometric means.

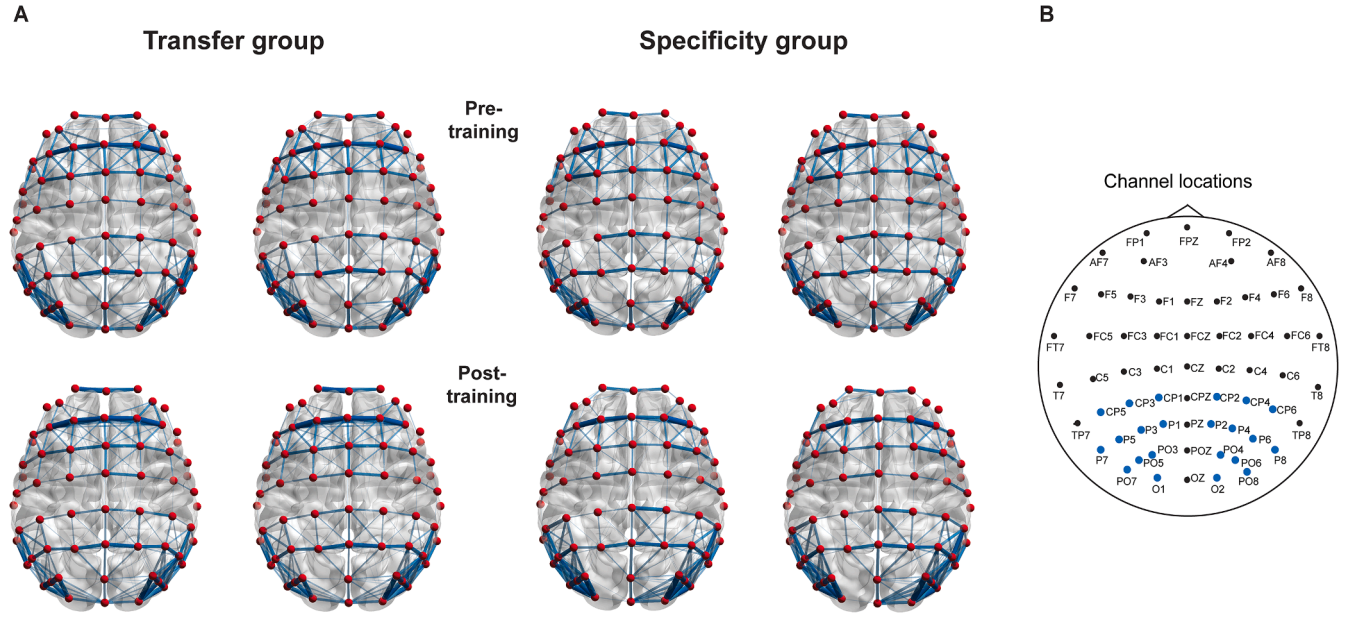

Fig. 4. Weighted functional connectivity graphs. **A.** Thresholded weighted PLV networks (sparsity = 0.10) for transfer and specificity groups pre- and post-training at trained (T_loc) and untrained (UT_loc) locations. Edge thickness reflects PLV strength. **B.** Topographical map of all EEG electrodes according to the standard 10–20 system. Blue solid circles indicate the posterior electrodes selected for analysis.

retain the strongest connections while preserving a sparse and interpretable network topology. Fig. 4A presents weighted functional connectivity graphs based on these thresholded matrices, where edge thickness reflects PLV strength and node positions correspond to standard electrode locations. This visualization reveals a distinct reorganization after training in the specificity group, which is characterized by locally denser and stronger connectivity among parieto-occipital electrodes (P1/3/5/7, PO3/5/7, O1, CP1/3/5 and their contralateral counterparts, Fig. 4B). This visual pattern suggested enhanced local segregation within the posterior network. To quantify this regional reorganization, we next examined network organization within the parieto-occipital subnetwork defined in Methods.

Weighted graphs were constructed using the original PLV values within this subnetwork. We first computed the average connection strength, defined as the mean PLV across all edges in the subnetwork, which provides an overall measure of the regional synchronization strength in the beta band. In addition, we quantified the average weighted clustering coefficient, which captures the tendency of nodes in this posterior network to form tightly interconnected local clusters, with strongly synchronized triads contributing more to the measure than weakly connected ones. Together, these two metrics offer complementary perspectives on training-related reorganization at the regional level, reflecting changes in both overall coupling strength and formation of locally specialized subnetworks (Fig. 5A-B). Separate LME analyses were performed on each of these measures with Training, Group, Location, and Hemisphere as fixed effects and Participant as a random intercept. The analysis of average weighted clustering coefficient revealed a significant main effect of Hemisphere ($F(1, 182) = 7.12$, $p = 0.008$, partial $\eta^2 = 0.04$), with weighted clustering generally higher in the left than in the right parieto-occipital subnetwork. A significant Group × Training interaction was also observed ($F(1, 182) = 6.47$, $p = 0.012$, partial $\eta^2 = 0.03$). Post hoc analysis with Bonferroni correction indicated that the specificity group exhibited higher weighted clustering coefficients after training ($t(182) = 2.11$, $p = 0.036$, *Cohen's d* = 0.40), which was not evident in the transfer group ($t(182) = -1.49$, $p = 0.137$, *Cohen's d* = −0.28). For the average connection strength, there was a significant main effect of Training ($F(1, 182) = 14.16$, $p < 0.001$, partial $\eta^2 = 0.07$) and a significant Group × Training interaction ($F(1, 182) = 8.35$, $p = 0.004$, partial $\eta^2 = 0.04$). Post hoc tests revealed that the specificity group exhibited significantly stronger average connection strength after training ($t(182) = 4.70$, $p < 0.001$, *Cohen's d* = 0.89), but the transfer group did not ($t(182) = 0.62$, $p = 0.538$, *Cohen's d* = 0.12). After training, the specificity group showed stronger mean connection strength and increased weighted clustering within the parieto-occipital network. Their concurrent increase indicated stronger and more locally concentrated posterior coupling, consistent with enhanced local specialization of visual processing. This regional pattern was also consistent with the whole-brain increases in aC and aL observed in the specificity group, suggesting a broader reorganization toward greater segregation and reduced integration.

4. Discussion

Our findings show that training-induced large-scale network reorganization is associated with whether perceptual learning remains location-specific or generalizes across retinal positions. Location-specific learners showed increased clustering coefficient together with longer characteristic path length, indicating stronger local segregation and reduced distributed integration (Fig. 3), whereas transfer learners showed comparatively stable network organization. These findings provide the first neural evidence that learning specificity is associated with a systems-level imbalance between local optimization and global integration. More broadly, they may also help understand learning specificity and transfer in other sensory modalities as well as other learning domains including motor, category, and memory learning.

The joint changes in clustering coefficient and characteristic path length provide a network-level explanation for specificity versus transfer. These two measures characterize complementary rather than opposing aspects of network organization. Increased clustering in the specificity group indicates stronger organization of neighboring nodes into locally interconnected groups, reflecting overly strengthened local

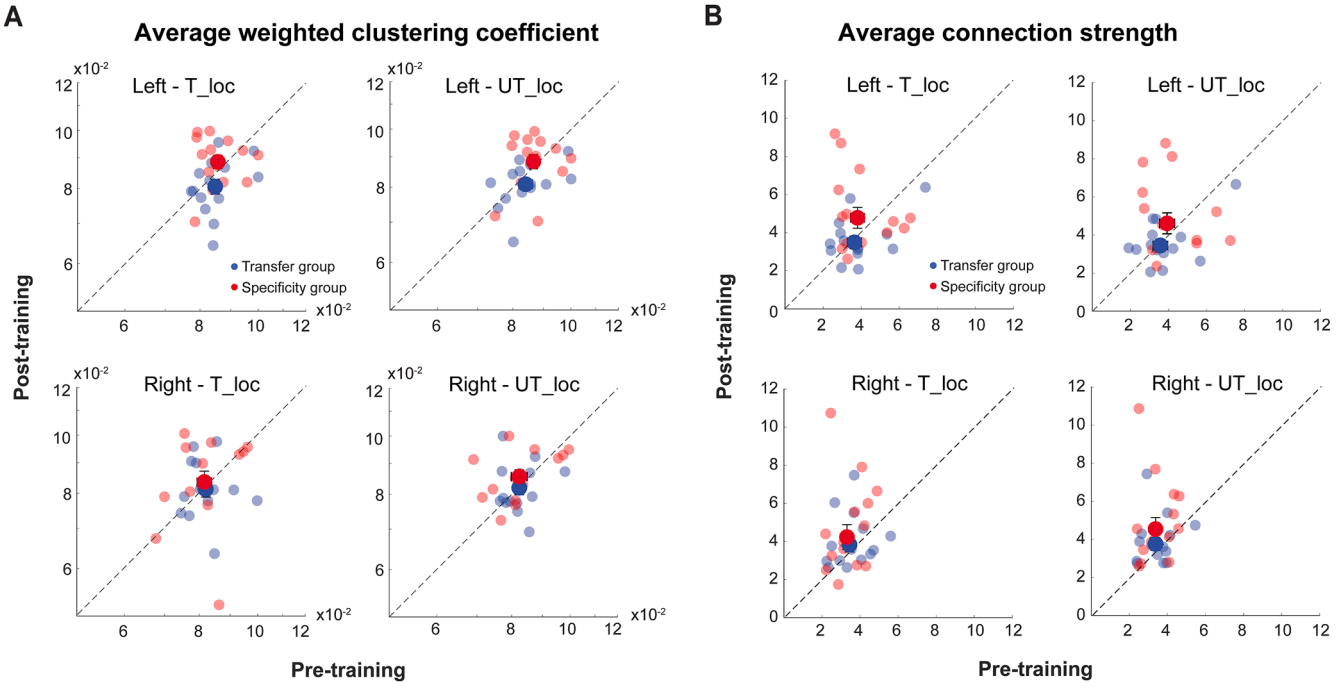

Fig. 5. Training-induced changes in local network properties within the parieto-occipital subnetwork. **A**. Average weighted clustering coefficient plotted separately for trained (T_loc) and untrained (UT_loc) locations in the left and right hemispheres. Small and large dots represent individual values and geometric means, respectively. **B**. Average connection strength.

processing and consistent with the overfitting hypothesis (Mollon and Danilova, 1996; Sagi, 2011). Such plasticity may become overly tuned to task-relevant and incidental features, reducing flexibility at new locations. The concurrent increase in characteristic path length indicates less efficient distributed communication, suggesting enhanced local segregation at the expense of global integration. In contrast, the transfer group maintained a more balanced organization. This interpretation also aligns with the connection-failure hypothesis, in which specificity results when higher-level learning mechanisms cannot effectively access sensory inputs representing untrained locations (Wang et al., 2012; Xiao et al., 2008; Xiong et al., 2016).

The posterior connectivity results further support this interpretation at a regional level (Fig. 5). The increases in connection strength and weighted clustering observed in the specificity group after training reflect stronger beta-band phase synchronization among posterior electrodes and more tightly interconnected local configurations, respectively (Lachaux et al., 1999; Rubinov and Sporns, 2010; Sauseng et al., 2005). Importantly, this stronger local synchronization does not imply more efficient global integration. The simultaneous increase in whole-brain characteristic path length indicates that stronger local organization coexisted with less efficient distributed integration (Rubinov and Sporns, 2010; Watts and Strogatz, 1998). At the regional level, weighted clustering was also generally higher in the left than in the right parieto-occipital subnetwork. Because no significant interaction involving Hemisphere was observed, this asymmetry appeared to be independent of the training-related group effect. Thus, the Group × Training effect was superimposed on a general left–right asymmetry rather than being selectively expressed in one hemisphere.

The spatial distribution of the network changes also helps reconcile the present findings with the ERP results from the same experiment. Zhang et al. (2013) found that training-related P1/N1 plasticity in the specificity group was confined to the trained location, with no significant modulation at the untrained location. In contrast, the present network analysis revealed broader bilateral reorganization of posterior functional connectivity (Figs. 4 and 5). These findings are not contradictory because ERP amplitudes and PLV-based measures reflect different aspects of neural processing: ERP components index stimulus-locked response changes, whereas PLV captures phase synchronization across distributed signals (Bullmore and Sporns, 2009; Stam et al., 2007). Thus, location-specific behavioral and ERP effects can coexist with broader network reorganization. Increased local clustering together with longer whole-brain characteristic path length suggests stronger segregation accompanied by reduced distributed integration, which may limit flexible coordination across locations.

The temporal stability of the graph measures across the task period further suggests that the observed network differences were not restricted to a brief stimulus-evoked interval. Instead, the relatively stable trajectories of clustering coefficient and characteristic path length are compatible with a sustained network configuration during task performance. Such sustained organization suggests that network dynamics were driven predominantly by top-down processes rather than bottom-up sensory changes. Top-down modulation is known to operate during both stimulus-present and stimulus-absent periods (Gazzaley and Nobre, 2012) and can stabilize large-scale network configurations (Bowling et al., 2020). Within this framework, the transfer group maintained a comparatively stable balance between local and distributed organization, whereas the specificity group showed a training-related shift toward stronger segregation and reduced integration. This difference may therefore reflect distinct network states associated with flexible versus location-bound expression of learning.

The beta band identified in the time-frequency analysis also formed the basis of the subsequent PLV network analysis. Beyond this role in network construction, beta activity itself showed a distinct training-related change in power. Posterior beta-band power decreased significantly after training in the specificity group, whereas no significant training-related change was detected in the transfer group. Beta activity has been associated with the maintenance of ongoing sensorimotor and cognitive states and with top-down processing of sensory information (Engel and Fries, 2010; Kilavik et al., 2013; Siegel et al., 2012). The reduction in beta power may therefore reflect a training-related change in the functional state of posterior visual systems, although its more specific functional meaning remains tentative because beta activity depends strongly on task and cortical context. Importantly, beta-power reductions in the specificity group occurred at both trained and untrained locations and over both ipsilateral and contralateral posterior electrodes. Their spatial distribution therefore did not parallel behavioral location specificity, suggesting a broader training-related change in posterior cortical state. Thus, oscillatory plasticity can extend beyond the spatial boundaries of behavioral specificity.

The network principles identified here may extend to other forms of learning in which both specificity and transfer are observed. In motor learning, improvements often fail to generalize across effectors or contexts (Donchin et al., 2003; Krakauer et al., 2000), but transfer can be promoted through double training (Yin et al., 2016). Category learning can likewise be retinal-specific yet become transferable under appropriate training conditions (Rosedahl et al., 2018; Zhu et al., 2026). These observations suggest that limited transfer need not reflect plasticity confined to local representations. Instead, excessive local optimization without sufficient global integration may constrain generalization across domains. The present graph-theoretical approach also complements ERP and fMRI studies emphasizing local amplitude or activation changes (Censor et al., 2009; Chang et al., 2014; Shibata et al., 2012; Zhang et al., 2013) by examining how learning-related changes are organized across distributed neural signals. Nevertheless, sensor-level EEG connectivity is limited by volume conduction and spatial resolution. Future multimodal and source-level studies, together with transfer-promoting paradigms such as double training, will be important for testing whether distributed network organization directly contributes to learning generalization.

Ethics statement

The study was approved by the Beijing Normal University Institutional Review Board. All participants provided informed consent prior to data collection.

Data and code availability

The data and code supporting the findings of this study will be made available upon request.

CRediT authorship contribution statement

Lin Zhong: Writing – original draft, Methodology, Data curation. **Gong-Liang Zhang:** Data curation. **Jun-Yun Zhang:** Conceptualization. **Cong Yu:** Writing – original draft, Conceptualization.

Declaration of competing interest

The authors declare no competing financial interests.

Acknowledgments

This work was supported by a National Natural Science Foundation of China, Brain Science and Brain-like Intelligence Technology – National Science and Technology Major Project grant (2022ZD0204600) to CY.

Appendix

Fig. A1.

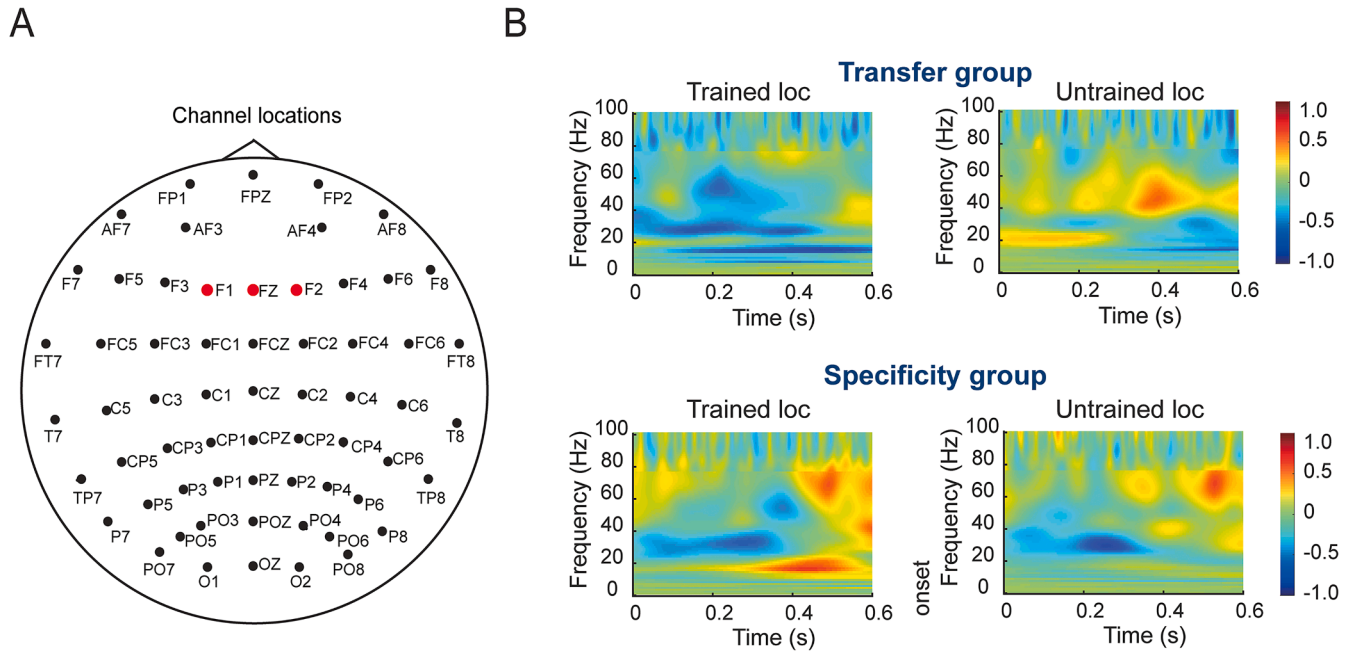

Fig. A.1. Frontal results. **A.** Topographical map of all EEG electrodes according to the standard 10–20 system. Red solid circles indicate the frontal electrodes selected for analysis. **B.** Time-frequency representations (1–100 Hz) show post- vs. pre-training power differences over frontal electrodes F1, F2 and FZ. Data include all 8 conditions: 2 groups × 2 hemispheres × 2 locations.

References

Achard, S., Bullmore, E., 2007. Efficiency and cost of economical brain functional networks. PLoS. Comput. Biol. 3 (2), e17. https://doi.org/10.1371/journal.pcbi.0030017.

Ahissar, M., Hochstein, S., 1997. Task difficulty and the specificity of perceptual learning. Nature 387 (6631), 401–406. https://doi.org/10.1038/41539.

Aydin, S., Onbasi, L., 2024. Graph theoretical brain connectivity measures to investigate neural correlates of music rhythms associated with fear and anger. Cogn. Neurodyn. 18 (1), 49–66. https://doi.org/10.1007/s11571-023-09931-5.

Aydın, S., 2024. Alzhemimer's disease is characterized by lower segregation in resting-State eyes-closed EEG. J. Med. Biol. Eng. 44 (6), 894–902. https://doi.org/10.1007/s40846-024-00917-0.

Aydın, S., Çetin, F.H., Uytun, M.Ç., Babadağî, Z., Güven, A.S., Işık, Y., 2022. Comparison of domain specific connectivity metrics for estimation brain network indices in boys with ADHD-C. Biomed. Signal. Process. Control 76, 103626. https://doi.org/10.1016/j.bspc.2022.103626.

Bates, D., Mächler, M., Bolker, B., Walker, S., 2015. Fitting linear mixed-effects models using lme4. J. Stat. Softw. 67 (1), 1–48. https://doi.org/10.18637/jss.v067.i01.

Bowling, J.T., Friston, K.J., Hopfinger, J.B., 2020. Top-down versus bottom-up attention differentially modulate frontal-parietal connectivity. Hum. Brain Mapp. 41 (4), 928–942. https://doi.org/10.1002/hbm.24850.

Bruns, A., Eckhorn, R., 2004. Task-related coupling from high- to low-frequency signals among visual cortical areas in human subdural recordings. Int. J. Psychophysiol. 51 (2), 97–116. https://doi.org/10.1016/j.ijpsycho.2003.07.001.

Bullmore, E., Sporns, O., 2009. Complex brain networks: graph theoretical analysis of structural and functional systems. Nat. Rev. Neurosci. 10 (3), 186–198. https://doi.org/10.1038/nrn2575.

Cai, L., Dong, Q., Wang, M., Niu, H., 2019. Functional near-infrared spectroscopy evidence for the development of topological asymmetry between hemispheric brain networks from childhood to adulthood. Neurophotonics 6 (2), 1. https://doi.org/10.1117/1.NPh.6.2.025005.

Censor, N., Bonneh, Y., Arieli, A., Sagi, D., 2009. Early-vision brain responses which predict human visual segmentation and learning. J. Vis. 9 (4), 12. https://doi.org/10.1167/9.4.12, 12.

Chang, D.H., Mevorach, C., Kourtzi, Z., Welchman, A.E., 2014. Training transfers the limits on perception from parietal to ventral cortex. Curr. Biol. 24 (20), 2445–2450. https://doi.org/10.1016/j.cub.2014.08.058.

Cohen, M.X., 2014. Analyzing Neural Time Series Data: Theory and Practice. The MIT Press. https://doi.org/10.7551/mitpress/9609.001.0001.

Crist, R.E., Kapadia, M.K., Westheimer, G., Gilbert, C.D., 1997. Perceptual learning of spatial localization: specificity for orientation, position, and context. J. Neurophysiol. 78 (6), 2889–2894. https://doi.org/10.1152/jn.1997.78.6.2889.

Delorme, A., Makeig, S., 2004. EEGLAB: an open source toolbox for analysis of single-trial EEG dynamics including independent component analysis. J. Neurosci. Methods 134 (1), 9–21. https://doi.org/10.1016/j.jneumeth.2003.10.009.

Di Russo, F., Martinez, A., Sereno, M.I., Pitzalis, S., Hillyard, S.A., 2002. Cortical sources of the early components of the visual evoked potential. Hum. Brain Mapp. 15 (2), 95–111. https://doi.org/10.1002/hbm.10010.

Ding, J., Sperling, G., Srinivasan, R., 2006. Attentional modulation of SSVEP power depends on the network tagged by the flicker frequency. Cereb. Cortex. 16 (7), 1016–1029. https://doi.org/10.1093/cercor/bhj044.

Donchin, O., Francis, J.T., Shadmehr, R., 2003. Quantifying generalization from trial-by-trial behavior of adaptive systems that learn with basis functions: theory and experiments in human motor control. J. Neurosci. 23 (27), 9032–9045. https://doi.org/10.1523/JNEUROSCI.23-27-09032.2003.

Donovan, I., Carrasco, M., 2018. Endogenous spatial attention during perceptual learning facilitates location transfer. J. Vis. 18 (11), 7. https://doi.org/10.1167/18.11.7.

Donovan, I., Szpiro, S.F., Carrasco, M., 2015. Exogenous attention facilitates location transfer of perceptual learning. J. Vis. 15 (10), 11. https://doi.org/10.1167/15.10.11, 11.

Engel, A.K., Fries, P., 2010. Beta-band oscillations–signalling the status quo? Curr. Opin. Neurobiol. 20 (2), 156–165. https://doi.org/10.1016/j.conb.2010.02.015.

Fahle, M., 1994. Human pattern-recognition - parallel-processing and perceptual-learning. Perception 23 (4), 411–427. https://doi.org/10.1068/p230411.

Fiorentini, A., Berardi, N., 1980. Perceptual learning specific for orientation and spatial frequency. Nature 287, 43–44. https://doi.org/10.1038/287043a0.

Garrison, K.A., Scheinost, D., Finn, E.S., Shen, X., Constable, R.T., 2015. The (in)stability of functional brain network measures across thresholds. Neuroimage 118, 651–661. https://doi.org/10.1016/j.neuroimage.2015.05.046.

Gazzaley, A., Nobre, A.C., 2012. Top-down modulation: bridging selective attention and working memory. Trends. Cogn. Sci. 16 (2), 129–135. https://doi.org/10.1016/j.tics.2011.11.014.

Harris, H., Gliksberg, M., Sagi, D., 2012. Generalized perceptual learning in the absence of sensory adaptation. Curr. Biol. 22 (19), 1813–1817. https://doi.org/10.1016/j.cub.2012.07.059.

Hu, D.Z., Wen, K., Chen, L.H., Yu, C., 2021. Perceptual learning evidence for supramodal representation of stimulus orientation at a conceptual level. Vis. Res. 187, 120–128. https://doi.org/10.1016/j.visres.2021.06.010.

Karni, A., Sagi, D., 1991. Where practice makes perfect in texture-discrimination - evidence for primary visual-cortex plasticity. Proc. Natl. Acad. Sci. U.S.A. 88 (11), 4966–4970. https://doi.org/10.1073/pnas.88.11.4966.

Kilavik, B.E., Zaepffel, M., Brovelli, A., MacKay, W.A., Riehle, A., 2013. The ups and downs of beta oscillations in sensorimotor cortex. Exp. Neurol. 245, 15–26. https://doi.org/10.1016/j.expneurol.2012.09.014.

Krakauer, J.W., Pine, Z.M., Ghilardi, M.F., Ghez, C., 2000. Learning of visuomotor transformations for vectorial planning of reaching trajectories. J. Neurosci. 20 (23), 8916–8924. https://doi.org/10.1523/JNEUROSCI.20-23-08916.2000.

Kuznetsova, A., Brockhoff, P.B., Christensen, R.H.B., 2017. lmerTest Package: tests in linear mixed effects models. J. Stat. Softw. 82 (13), 1–26. https://doi.org/10.18637/jss.v082.i13.

Lachaux, J.-P., Rodriguez, E., Martinerie, J., Varela, F.J., 1999. Measuring phase synchrony in brain signals. Hum. Brain Mapp. 8 (4), 194–208. https://doi.org/10.1002/(sici)1097-0193(1999)8. :4<194::Aid−bm4>3.0.Co;2-c.

Lenth, R.V., Piaskowski, J., 2025. emmeans: estimated Marginal means, aka Least-Squares means. https://rvlenth.github.io/emmeans/.

Mangun, G.R., Hillyard, S.A., 1991. Modulations of sensory-evoked brain potentials indicate changes in perceptual processing during visual-spatial priming. J. Exp. Psychol. Hum. Percept. Perform. 17 (4), 1057–1074. https://doi.org/10.1037//0096-1523.17.4.1057.

Maris, E., Oostenveld, R., 2007. Nonparametric statistical testing of EEG- and MEG-data. J. Neurosci. Methods 164 (1), 177–190. https://doi.org/10.1016/j.jneumeth.2007.03.024.

Mastropasqua, T., Galliussi, J., Pascucci, D., Turatto, M., 2015. Location transfer of perceptual learning: passive stimulation and double training. Vis. Res 108, 93–102. https://doi.org/10.1016/j.visres.2015.01.024.

Mollon, J.D., Danilova, M.V., 1996. Three remarks on perceptual learning. Spat. Vis. 10 (1), 51–58. https://doi.org/10.1163/156856896X00051.

Onnela, J.-P., Saramäki, J., Kertész, J., Kaski, K., 2005. Intensity and coherence of motifs in weighted complex networks. Phys. Rev. E 71 (6). https://doi.org/10.1103/physreve.71.065103.

Oostenveld, R., Fries, P., Maris, E., Schoffelen, J.M., 2011. FieldTrip: open source software for advanced analysis of MEG, EEG, and invasive electrophysiological data. Comput. Intell. Neurosci. 2011, 156869. https://doi.org/10.1155/2011/156869.

Perrin, F., Pernier, J., Bertrand, O., Echallier, J.F., 1989. Spherical splines for scalp potential and current density mapping. Electroencephalogr. Clin. Neurophysiol. 72 (2), 184–187. https://doi.org/10.1016/0013-4694(89)90180-6.

Rosedahl, L.A., Eckstein, M.P., Ashby, F.G., 2018. Retinal-specific category learning. Nat. Hum. Behav. 2 (7), 500–506. https://doi.org/10.1038/s41562-018-0370-z.

Rubinov, M., Sporns, O., 2010. Complex network measures of brain connectivity: uses and interpretations. Neuroimage 52 (3), 1059–1069. https://doi.org/10.1016/j.neuroimage.2009.10.003.

Sagi, D., 2011. Perceptual learning in Vision research. Vis. Res. 51 (13), 1552–1566. https://doi.org/10.1016/j.visres.2010.10.019.

Sauseng, P., Klimesch, W., Schabus, M., Doppelmayr, M., 2005. Fronto-parietal EEG coherence in theta and upper alpha reflect central executive functions of working memory. Int. J. Psychophysiol. 57 (2), 97–103. https://doi.org/10.1016/j.ijpsycho.2005.03.018.

Schoups, A., Vogels, R., Orban, G.A., 1995. Human perceptual learning in identifying the oblique orientation: retinotopy, orientation specificity and monocularity. J. Physiol. 483 (Pt 3), 797–810. https://doi.org/10.1113/jphysiol.1995.sp020623.

Shibata, K., Chang, L.H., Kim, D., Nanez Sr., J.E., Kamitani, Y., Watanabe, T., Sasaki, Y., 2012. Decoding reveals plasticity in V3A as a result of motion perceptual learning. PLoS. One 7 (8), e44003. https://doi.org/10.1371/journal.pone.0044003.

Siegel, M., Donner, T.H., Engel, A.K., 2012. Spectral fingerprints of large-scale neuronal interactions. Nat. Rev. Neurosci. 13 (2), 121–134. https://doi.org/10.1038/nrn3137.

Sporns, O., 2013. Network attributes for segregation and integration in the human brain. Curr. Opin. Neurobiol. 23 (2), 162–171. https://doi.org/10.1016/j.conb.2012.11.015.

Stam, C.J., Nolte, G., Daffertshofer, A., 2007. Phase lag index: assessment of functional connectivity from multi channel EEG and MEG with diminished bias from common sources. Hum. Brain Mapp. 28 (11), 1178–1193. https://doi.org/10.1002/hbm.20346.

van Driel, J., Gunseli, E., Meeter, M., Olivers, C.N.L., 2017. Local and interregional alpha EEG dynamics dissociate between memory for search and memory for recognition. Neuroimage 149, 114–128. https://doi.org/10.1016/j.neuroimage.2017.01.031.

Wang, J., Wang, X., Xia, M., Liao, X., Evans, A., He, Y., 2015. GRETNA: a graph theoretical network analysis toolbox for imaging connectomics. Front. Hum. Neurosci. 9, 386. https://doi.org/10.3389/fnhum.2015.00386.

Wang, R., Cong, L.J., Yu, C., 2013. The classical TDT perceptual learning is mostly temporal learning. J. Vis. 13 (5), 1–9. https://doi.org/10.1167/13.5.9. *9*.

Wang, R., Wang, J., Zhang, J.Y., Xie, X.Y., Yang, Y.X., Luo, S.H., Yu, C., Li, W., 2016. Perceptual learning at a conceptual level. J. Neurosci. 36 (7), 2238–2246. https://doi.org/10.1523/JNEUROSCI.2732-15.2016.

Wang, R., Zhang, J.Y., Klein, S.A., Levi, D.M., Yu, C., 2012. Task relevancy and demand modulate double-training enabled transfer of perceptual learning. Vis. Res. 61, 33–38. https://doi.org/10.1016/j.visres.2011.07.019.

Wang, R., Zhang, J.Y., Klein, S.A., Levi, D.M., Yu, C., 2014. Vernier perceptual learning transfers to completely untrained retinal locations after double training: a "piggybacking" effect. J. Vis. 14 (13), 12. https://doi.org/10.1167/14.13.12. *12*.

Watts, D.J., Strogatz, S.H., 1998. Collective dynamics of 'small-world' networks. Nature 393 (6684), 440–442. https://doi.org/10.1038/30918.

Xiao, L.Q., Zhang, J.Y., Wang, R., Klein, S.A., Levi, D.M., Yu, C., 2008. Complete transfer of perceptual learning across retinal locations enabled by double training. Curr. Biol. 18 (24), 1922–1926. https://doi.org/10.1016/j.cub.2008.10.030.

Xiong, Y.Z., Guan, S.C., Yu, C., 2022. A supramodal and conceptual representation of subsecond time revealed with perceptual learning of temporal interval discrimination. Sci. Rep. 12 (1), 10668. https://doi.org/10.1038/s41598-022-14698-6.

Xiong, Y.Z., Zhang, J.Y., Yu, C., 2016. Bottom-up and top-down influences at untrained conditions determine perceptual learning specificity and transfer. Elife 5 (14614), 1–17. https://doi.org/10.7554/eLife.14614.

Yin, C., Bi, Y., Yu, C., Wei, K., 2016. Eliminating direction specificity in visuomotor learning. J. Neurosci. 36 (13), 3839–3847. https://doi.org/10.1523/JNEUROSCI.2712-15.2016.

Yu, C., Klein, S.A., Levi, D.M., 2004. Perceptual learning in contrast discrimination and the (minimal) role of context. J. Vis. 4 (3), 4. https://doi.org/10.1167/4.3.4.

Zhang, G.L., Cong, L.J., Song, Y., Yu, C., 2013. ERP P1-N1 changes associated with vernier perceptual learning and its location specificity and transfer. J. Vis. 13 (4). https://doi.org/10.1167/13.4.19. *19*.

Zhang, J.Y., Zhang, G.L., Xiao, L.Q., Klein, S.A., Levi, D.M., Yu, C., 2010. Rule-based learning explains visual perceptual learning and its specificity and transfer. J. Neurosci. 30 (37), 12323–12328. https://doi.org/10.1523/JNEUROSCI.0704-10.2010.

Zhu, J.P., Xie, X.Y., Yu, C., Zhang, J.Y., 2026. Double training promotes retinotopic transfer of category learning. NPJ. Sci. Learn. 11. https://doi.org/10.1038/s41539-025-00396-1.